Nanoscale

PAPER

View Article Online
View Journal | View Issue

Core–shell-like Y_2O_3:[(Tb^{3+}–Yb^{3+}), Li^+]/CdZnS heterostructure synthesized by super-close-space sublimation for broadband down-conversion

Cite this: *Nanoscale*, 2014, **6**, 4745

Xiaojie Wu,[a] Zhenzhong Zhang,*[b] Fanzhi Meng,[a] Yingning Yu,[a] Lin Han,[a] Xiaojuan Liu[a] and Jian Meng*[a]

Received 14th December 2013
Accepted 20th January 2014

DOI: 10.1039/c3nr06625h

www.rsc.org/nanoscale

Combination with semiconductors is a promising approach to the realization of broadband excitation of light conversion materials based on rare earth compounds, to boost the energy efficiency of silicon solar cells. $Cd_{1-x}Zn_xS$ is a wide bandgap semiconductor with large exciton binding energy. By changing its composition, the bandgap of $Cd_{1-x}Zn_xS$ can be tuned to match the absorption of trivalent lanthanide (Ln) ions, which makes it a competent energy donor for the Ln^{3+}–Yb^{3+} couple. In this work, we designed a clean route to a broadband down-converter based on a core–shell-like Y_2O_3:[(Tb^{3+}–Yb^{3+}), Li^+]/$Cd_{0.81}Zn_{0.19}S$ (CdZnS) heterostructure. By hot-pressing and subsequent annealing of a Y_2O_3:[(Tb^{3+}–Yb^{3+}), Li^+]/CdZnS mixture, highly pure CdZnS was sublimated and deposited on the Y_2O_3:[(Tb^{3+}–Yb^{3+}), Li^+] grains while maintaining the original composition of the precursor. The CdZnS shell acted as a light absorber and energy donor for the Tb^{3+}–Yb^{3+} quantum cutting couple. Because the use of solvents was avoided during the formation of the heterostructures, few impurities were incorporated into the samples, and the non-radiative transition was therefore markedly suppressed. The Y_2O_3:[(Tb^{3+}–Yb^{3+}), Li^+]/CdZnS heterostructures possess strong near-infrared (NIR) luminescence from Yb^{3+}. Broadband down-conversion to the Yb^{3+} NIR emission was obtained in a wide range of 250–650 nm.

Semiconductor–rare earth composites can combine the strong and broad absorption of semiconductors with the sharp and narrow emission of rare earth materials. Because of their applications in light conversion, such as for solar cells and light emitting devices, light converters based on these materials have attracted increasing interest in recent years.[1–5] The small solid solubility of rare earth ions in semiconductors means that it is more feasible to synthesize multiphase composites than single-phase rare-earth doped semiconductor materials. Such multi-phase materials, including core–shell structures and quantum dot doped glass structures, have been widely and deeply studied. Compared with quantum dot doped glass, core–shell materials possess stronger light absorption owing to their large light receiving area. In general, most phosphor–semiconductor core–shell materials are synthesized in solvents,[6] where some impurities will be inevitably introduced. It impacts on the luminescence performance of both the semiconductor and the rare earth ions. In particular, for some Yb^{3+}-based light emitters with luminescence energies of about 10 000 cm^{-1}, contaminants like C–H and O–H, which possess high vibration energies of about 3000 cm^{-1}, can easily cause luminescence quenching.[1] Therefore, it is beneficial and necessary to develop a clean route to rare earth–semiconductor core–shell light emitters and/or converters. In this work, hot-pressing and subsequent thermal annealing were used to fabricate core–shell-like Y_2O_3:[(Tb^{3+}–Yb^{3+}), Li^+]/CdZnS heterostructures. Quantum cutting down-conversion based on Yb has been widely studied.[7–12] In the Tb^{3+}–Yb^{3+} quantum cutting couple, one blue photon is absorbed through the $^7F_6$–$^5D_4$ transition of Tb^{3+}, and cut into two near-infrared (NIR) photons from Yb^{3+}.[7–10] $Cd_{1-x}Zn_xS$ possesses a tunable bandgap (2.4–3.6 eV) and a large exciton binding energy, which is conducive to the efficient energy transfer (ET) to rare earth ions. A strong emission around 980 nm was obtained under broadband excitation in the range from 250 to 650 nm. This emission is located at the maximum spectral response (~1000 nm) of silicon solar cells. Because the present down-converter can partly reduce the spectral mismatch between sunlight and the spectral response of silicon, it is expected to boost the energy conversion efficiency of silicon solar cells.

At first, the Y_2O_3:[(Tb^{3+}–Yb^{3+}), Li^+]/$Cd_{0.81}Zn_{0.19}S$ (CdZnS) composites in a mole ratio of 80 : 20 were fabricated by a hot-pressing method on a spark plasma sintering (SPS) system. The Y_2O_3:[(Tb^{3+}–Yb^{3+}), Li^+] phosphor powder, with a size of

[a]*State Key Laboratory of Rare Earth Resources Utilization, Changchun Institute of Applied Chemistry, Chinese Academy of Sciences, 5625 Renmin Street, Changchun 130022, People's Republic of China. E-mail: jmeng@ciac.jl.cn*

[b]*State Key Laboratory of Luminescence and Applications, Changchun Institute of Optics, Fine Mechanics and Physics, Chinese Academy of Sciences, 3888 Dongnanhu Road, Changchun 130033, People's Republic of China. E-mail: zhangzz@ciomp.ac.cn*

100–200 nm, was prepared as one of the precursors by a sol–gel method. 2 mol% Li^+ ions, which have smaller ionic radii, were used to reduce the site symmetry of the local environment surrounding the Ln^{3+} ions. This enhances the cross-section of the intra-4f transitions.[13] The obtained phosphor powder was vacuum annealed at 1000 °C for 1.5 hours to suppress the formation of Tb^{4+} and the resulting Tb^{4+}–Yb^{2+} charge transfer state.[14] CdZnS powder, with a size of 2–4 μm, as the other precursor was synthesized by a solid sintering method by mixing 99.999% CdS and 99.999% ZnS. The composition was optimized at $Cd_{0.81}Zn_{0.19}S$ to make the bandgap match the $^5D_4 \rightarrow {}^7F_6$ absorption of Tb^{3+} ions. The two precursor powders were finely milled together in an argon atmosphere to ensure uniform mixing, and were then compacted in a hard alloy die at 550 °C for 10 minutes. In the meantime, a uniaxial pressure of 150 MPa was applied on the samples to reduce the space among the precursor grains. Finally, the shaped two-phase samples were annealed in argon at about 850–950 °C. A graphite package was used to protect the samples from volatilization loss or oxidation. During this annealing process, some atoms will be sublimated from the CdZnS grains and deposited on the phosphor grain surface to form the core–shell-like heterostructures. In general, composition segregation is apt to take place in an alloy grown by vapor deposition due to the vapor pressure difference between the components. Hot pressing markedly reduces the space among the precursor grains, which suppresses the composition segregation of the deposited CdZnS. X-ray diffraction (XRD) was performed on a Rigaku D/Max 2500 diffractometer using Cu Kα radiation (0.15405 nm) operated at 40 kV and 200 mA. The XRD patterns for Rietveld refinement were recorded from 10° to 110° in steps of 0.02° with a counting time of 2 s per step. The Rietveld refinement was performed using a GSAS-EXPGUI program. The morphology was studied by using a Hitachi S-4800 scanning electron microscope and a JEOL JEM-2010 transmission electron microscope. The photoluminescence (PL) emission and excitation spectra were measured on an FLSP 920 spectrometer. The photoluminescence decay curves were recorded using a Lecroy Wave Runner 6100 digital oscilloscope (1 GHz). A tunable laser (Continuum Sunlite OPO) with a pulse width of 4 ns was used as the excitation source.

Fig. 1(A) shows the XRD pattern of the single $(Y_{0.89}Tb_{0.01}Yb_{0.08}Li_{0.02})_2O_3$ phosphor after hot-pressing, with Rietveld refinements. The samples were indexed to the cubic bixbyite Y_2O_3 structure, within space-group $Ia\bar{3}$ (Th7) (no. 206). The Tb and Yb atoms randomly occupy the two types of cationic substitution sites with point symmetry S_6 and C_2 in the Y_2O_3 lattice. The Rietveld refinement demonstrates that the phosphor maintained its cubic Y_2O_3 structure after hot-pressing in our experiments. Fig. 1(B) shows a typical XRD pattern of the CdZnS/$(Y_{0.89}Tb_{0.01}Yb_{0.08}Li_{0.02})_2O_3$ heterostructures. The pink bars represent angular positions of the possible Bragg diffractions for the $(Y_{0.89}Tb_{0.01}Yb_{0.08}Li_{0.02})_2O_3$ phase, extracted from Fig. 1(A). The labeled positions agree well with the diffractions of the $(Y_{0.89}Tb_{0.01}Yb_{0.08}Li_{0.02})_2O_3$ phase in the heterostructures. The other peaks, labeled with blue dots, show a slight shift to a large-angle side compared with the diffractions of hexagonal

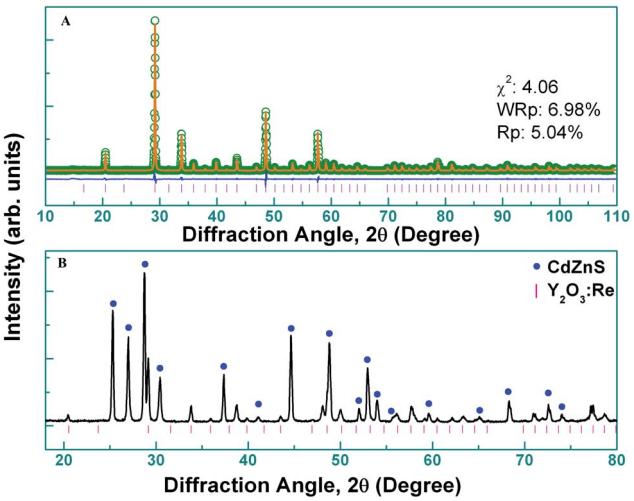

Fig. 1 (A) XRD spectra of the $(Y_{0.89}Tb_{0.01}Yb_{0.08}Li_{0.02})_2O_3$ after hot-pressing. The green circles denote experimental data, and the orange lines are the calculated curves. The pink bars represent the angular positions of the possible Bragg diffractions for the hot-pressed $(Y_{0.89}Tb_{0.01}Yb_{0.08}Li_{0.02})_2O_3$. The difference between the measured and calculated intensity is depicted by the blue line at the bottom. (B) The XRD pattern of the core–shell-like CdZnS/$(Y_{0.89}Tb_{0.01}Yb_{0.08}Li_{0.02})_2O_3$ heterostructures demonstrates that the samples are composed of only CdZnS and $(Y_{0.89}Tb_{0.01}Yb_{0.08}Li_{0.02})_2O_3$ phases with a cubic bixbyite Y_2O_3 structure.

CdS reported in JCPDS (#75-1545, #77-2306). Considering the incorporation of Zn into the lattice, they are assigned to the diffractions of a $Cd_{0.81}Zn_{0.19}S$ phase. No diffraction peaks from any other phase were observed. That is, the composite was composed of only hexagonal CdZnS and Y_2O_3:[(Tb^{3+}–Yb^{3+}), Li^+] with a cubic bixbyite Y_2O_3 structure.

After hot-pressing at 150 MPa, the apparent volume of the composite decreased by about 13% compared with that after pre-pressing at only 25 MPa. This was due to the reduction of the space among the precursor grains. Fig. 2(A) is a top-view SEM image of the samples, which shows that small grains were distributed on the boundaries of the larger grains. The two types of grains were of the phosphor and CdZnS phases, respectively, according to the size of the precursors. TEM images of the fragments milled off from the final samples are shown in Fig. 2(B) and (C), in which it is clear that the samples possessed core–shell-like structures. Fig. 2(E) to (G) show energy-dispersive X-ray (EDX) spectroscopy images of the samples. Fig. 2(D) is the dark field image of a core–shell-like grain. The intensity of the K-lines of Y, Cd and S are represented by the brightness, which was used to reflect the distribution of these elements as shown in Fig. 2(E–G). The Y atoms were concentrated in the grain interior, while the Cd and S atoms were enriched on the grain surface. This clearly indicates the formation of a [phosphor core]–[CdZnS shell] heterostructure.

Fig. 3 shows TEM images of the samples before and after the final annealing. After annealing at 920 °C, the phosphor grains possessed a much thicker CdZnS shell than that prior to annealing. This indicates that the core–shell-like structure was mainly formed during the final annealing process by vapor

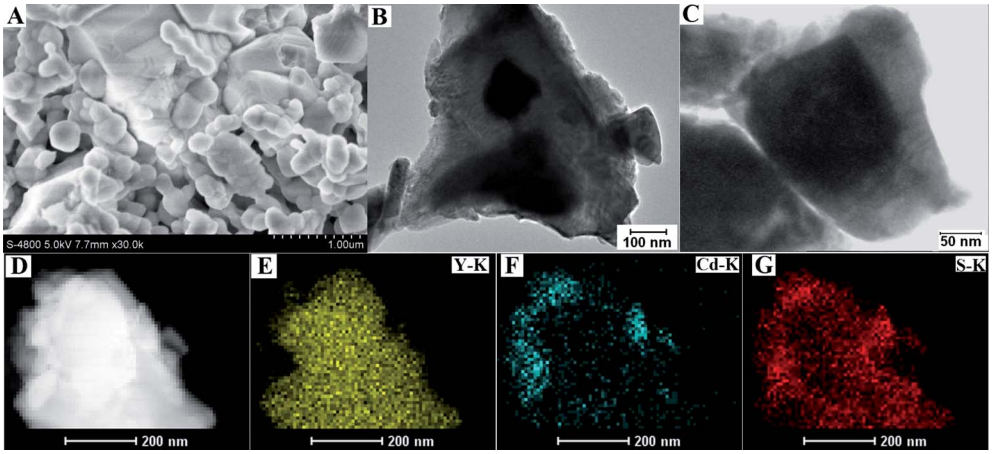

Fig. 2 (A) An SEM image of the samples. (B) and (C) TEM images of a final sample after milling. (D) A TEM dark field image and (E)–(G) EDX spectroscopy images of a grain, indicating the formation of core–shell-like Y_2O_3:[(Tb^{3+}–Yb^{3+}), Li^+]/CdZnS heterostructures.

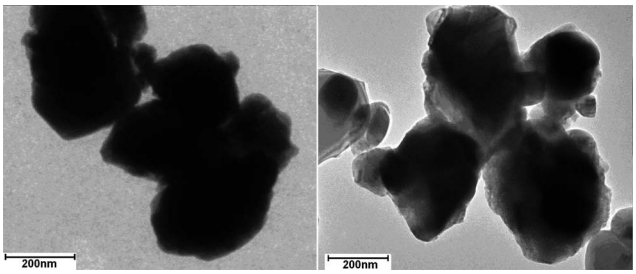

Fig. 3 TEM images of the fractions milled from the sample before and after the final annealing.

deposition. No doubt, the CdZnS shell formed by high temperature deposition possesses better crystal quality than the CdZnS powder precursor.

The PL emission spectra of Yb^{3+} in the $(Y_{0.89}Yb_{0.08}Tb_{0.01}Li_{0.02})_2O_3$/CdZnS core–shell-like heterostructures are shown in Fig. 4(A). The sample showed a strong NIR emission in the region of 850–1150 nm, which resulted from the $^2F_{5/2} \rightarrow {}^2F_{7/2}$ transitions of Yb^{3+}. The emission under excitation at 472 nm exhibited much stronger intensity than that under excitation at 300 nm. Fig. 4(B) shows the excitation spectra of the single $(Y_{0.89}Yb_{0.08}Tb_{0.01}Li_{0.02})_2O_3$ phosphor and the core–shell-like $(Y_{0.89}Yb_{0.08}Tb_{0.01}Li_{0.02})_2O_3$/CdZnS heterostructures, in black and blue, respectively, obtained by monitoring the NIR emission at 976 nm. The single phosphor showed an excitation band mainly located in the UV region, resulting from the $4f^75d^1$ state absorption of Tb^{3+}. In contrast, a broad excitation band, which covered a region from 250 to 650 nm, was observed for the core–shell-like heterostructures. The emission intensity under visible excitation was always larger than that under UV excitation. The maximum was located at 472 nm, corresponding to the absorption edge of $Cd_{0.81}Zn_{0.19}S$. Note that the excitation band was extended to 650 nm, the corresponding energy of which is smaller than the bandgap of $Cd_{0.81}Zn_{0.19}S$. The excitation with lower energy than the $Cd_{0.81}Zn_{0.19}S$ bandgap should be mainly caused by the absorption of defects in $Cd_{0.81}Zn_{0.19}S$. The down-conversion in this region should be caused by the energy transition from defect levels of CdZnS to one Yb^{3+} ion, rather than the quantum cutting process. It is very significant for practical applications that the excitation band covers the visible region. It is known that sunlight that reaches the ground is not equal-energy white light. It contains 44% visible light, which is much greater than the ultraviolet contribution of 3%.[15,16] The excitation result under sunlight should be depicted by "corrected" excitation spectra, which are the product of the excitation spectra and the normalized solar spectrum, as shown in Fig. 4(C). The normalized solar spectrum from 200 nm to 700 nm is also shown in Fig. 4(C), in orange. Here, because the excitation spectra of the core–shell-like $(Y_{0.89}Yb_{0.08}Tb_{0.01}Li_{0.02})_2O_3$/CdZnS heterostructures and single $(Y_{0.89}Yb_{0.08}Tb_{0.01}Li_{0.02})_2O_3$ phosphor are recorded under the same conditions, their intensity ratios

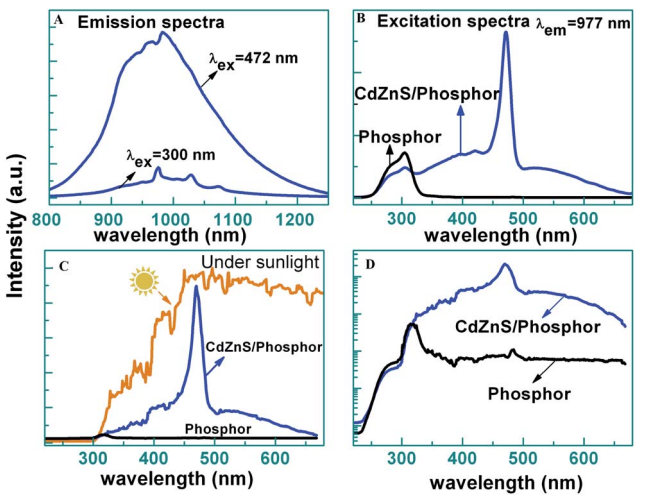

Fig. 4 (A) NIR emission spectra (λ_{ex} = 300 nm, 472 nm) of the core–shell-like $(Y_{0.89}Yb_{0.08}Tb_{0.01}Li_{0.02})_2O_3$/CdZnS heterostructures. (B) Excitation spectra (λ_{em} = 976 nm) of the heterostructures and the single $(Y_{0.89}Yb_{0.08}Tb_{0.01}Li_{0.02})_2O_3$ phosphor. (C) Excitation spectra multiplied by the normalized solar spectrum. (D) Comparison between the "corrected" excitation spectra. The intensity is logarithmic.

reflect the difference in luminescence performance between the two materials. It is clear that the area under the "corrected" excitation spectrum curve of the core–shell-like ZnCdS/$(Y_{0.89}Yb_{0.08}Tb_{0.01}Li_{0.02})_2O_3$ heterostructures (colored in blue) is much larger than that of the single phosphor (in black). To show the discrepancy in down-conversion effect more clearly, the curves in Fig. 4(C) were redrawn using a logarithmic scale in Fig. 4(D). A marked improvement approaching two orders of magnitude is observed.

A $(Y_{0.89}Yb_{0.08}Tb_{0.01}Li_{0.02})_2O_3$/ZnO sample was synthesized through the same process to investigate whether the broadening of the excitation band of 977 nm emission was caused by compositing with semiconductor. Fig. 5(A) shows the diffuse reflectance spectra of phosphors combined with ZnO and the CdZnS semiconductor, respectively. Clear absorption edges were observed in accordance with the bandgaps of bulk ZnO (3.2 eV) and $Cd_{0.81}Zn_{0.19}S$ (2.6 eV). The absorption between 900 and 1050 nm is caused by the transition of Yb^{3+} $^2F_{7/2} \rightarrow {}^2F_{5/2}$. Fig. 5(B) shows the excitation spectra of Yb^{3+} emission at 977 nm in the single $(Y_{0.89}Yb_{0.08}Tb_{0.01}Li_{0.02})_2O_3$ phosphor and the core–shell-like $(Y_{0.89}Yb_{0.08}Tb_{0.01}Li_{0.02})_2O_3$/semiconductor structures. The emission intensity is normalized for a clear comparison. For the single phosphor, which was not combined with any semiconductor, the emission intensity decreased abruptly as the excitation wavelength exceeded 310 nm. The excitation peak at 484 nm was much weaker than the peak observed in the UV region. In contrast, the phosphor–semiconductor samples showed much broader excitation bands. Besides the 300 nm excitation peak, excitation peaks at 388 and 472 nm were observed, in agreement with the absorption edges of ZnO and $Cd_{0.81}Zn_{0.19}S$, respectively. The excitation spectra maintained considerable intensity between the UV peak and the lower-energy excitation peak. That is, the broadening of the excitation band originated from the combination with the semiconductor.

To investigate the role of Tb ions in energy transfer (ET) processes in the core–shell-like phosphor/CdZnS heterostructures, an excitation spectrum of a sample without Tb doping (the orange curve) was also recorded, as shown in Fig. 5(C), which has been multiplied by 10 for a clearer comparison. The Yb^{3+} $^2F_{5/2} \rightarrow {}^2F_{7/2}$ emission intensity decreased markedly when the Tb fraction was absent. This means that the Tb ions acted as a bridge between CdZnS and Yb^{3+}. The PL time decay of the Tb^{3+} $^5D_4$ level in the core–shell-like Y_2O_3:[(Tb^{3+}–Yb^{3+}), Li^+]/CdZnS heterostructures was measured to calculate the energy transfer efficiency (ETE) in the Tb^{3+}–Yb^{3+} couple, as shown in Fig. 5(D). In these samples, the Yb^{3+} concentration was increased from 0 to 10 mol%, while the content of Tb was fixed at 1 mol%. The excitation wavelength was 483 nm and the monitoring wavelength was 544 nm. The lifetime decreased monotonically from 1.103 ms to 0.45 ms with increasing Yb^{3+} fractions from 0.00 to 0.10. This supports the occurrence of ET from the Tb^{3+} ions to the Yb^{3+} ions. The corresponding ETE is up to 51.8% at a Yb^{3+} fraction of 0.08, calculated using the expression $\mathrm{ETE} = 1 - \dfrac{\int I_{x(\mathrm{Yb})}\,\mathrm{d}t}{\int I_{0(\mathrm{Yb})}\,\mathrm{d}t}$, where $I_{x(\mathrm{Yb})}$ and $I_{0(\mathrm{Yb})}$ are the luminescence intensity as a function of time t for Yb^{3+} concentration $= x$ and 0.[7] Considering the quantum cutting effect in the Tb^{3+}–Yb^{3+} couple,[7–10] the corresponding NIR quantum efficiency of down-conversion was calculated to be 151.8%.[7]

A diagram of the ET process in the core–shell-like Y_2O_3:[(Tb^{3+}–Yb^{3+}), Li^+]/CdZnS heterostructures is shown in Fig. 6. The CdZnS phase absorbs the high-energy photons through band-to-band transitions, then relaxes the photogenerated carriers to its band edge and some defect levels, and finally sensitizes the Yb^{3+} $^2F_{5/2} \rightarrow {}^2F_{7/2}$ emission through the bridge effect of the Tb^{3+} $^5D_4 \rightarrow {}^7F_6$ transition. In other words, the ET process was mainly composed

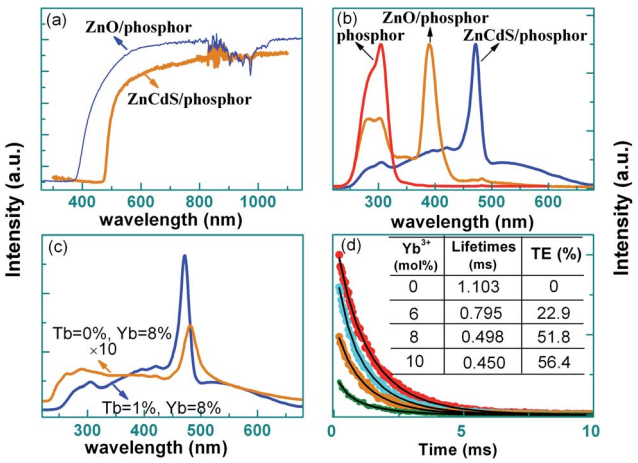

Fig. 5 (A) Diffuse reflectance spectra of $(Y_{0.89}Yb_{0.08}Tb_{0.01}Li_{0.02})_2O_3$/ZnO and $(Y_{0.89}Yb_{0.08}Tb_{0.01}Li_{0.02})_2O_3$/ZnCdS, respectively. (B) Excitation spectra of the single $(Y_{0.89}Yb_{0.08}Tb_{0.01}Li_{0.02})_2O_3$, the $(Y_{0.89}Yb_{0.08}Tb_{0.01}Li_{0.02})_2O_3$/ZnO, and $(Y_{0.89}Yb_{0.08}Tb_{0.01}Li_{0.02})_2O_3$/CdZnS heterostructures. (C) Excitation spectra comparison between the samples with and without Tb doping. The content of Tb and Yb in the phosphor phase were (Tb = 0.01, Yb = 0.08) (blue) and (Tb = 0.00, Yb = 0.08) (orange), respectively. (D) Luminescence decay curves of Tb^{3+} 544 nm emission in the core–shell. (Tb = 0.01, Yb = 0.00, 0.06, 0.08 and 0.10).

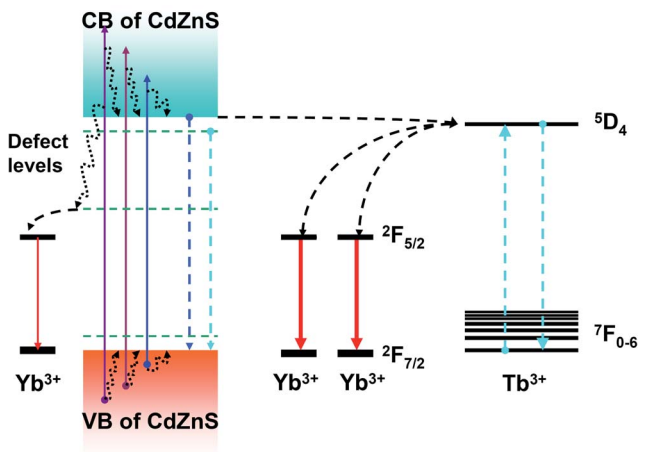

Fig. 6 A diagram of the ET in the core–shell-like Y_2O_3:[(Tb^{3+}–Yb^{3+}), Li^+]/CdZnS heterostructures.

of the transfer from CdZnS to Tb^{3+}, and the subsequent QC down-conversion in the Tb^{3+}–Yb^{3+} couple. For the other channel, the direct ET process from defect levels in CdZnS and Yb^{3+} ions played only a small part.

In summary, we have reported a super-close-space sublimation method for the synthesis of core–shell-like Y_2O_3:[(Tb^{3+}–Yb^{3+}), Li^+]/$Cd_{0.81}Zn_{0.19}S$ heterostructures, using hot-pressing and subsequent annealing processes. Benefitting from the extremely close space in the sample caused by hot-pressing, CdZnS shells with high purity and unchanged composition were deposited on the phosphor core. In contrast to wet chemical routes, this clean route introduces few quenching centers, and is therefore conducive to increased luminescence efficiency. Efficient energy transfer from CdZnS to the Tb^{3+}–Yb^{3+} QC couple was demonstrated, and broadband down-conversion (250–650 nm) to Yb^{3+} emission at around 1000 nm was realized. These results are expected to be applied to boost the energy efficiency of silicon solar cells.

Acknowledgements

This work is supported by the National Natural Science Foundation of China under Grants nos 51002148, 51372244, 21221061 and 21071141, and by the Natural Science Foundation of Jilin province, China, under grant no. 201115126.

Notes and references

1 R. Martín-Rodríguez, R. Geitenbeek and A. Meijerink, *J. Am. Chem. Soc.*, 2013, **135**, 13668.
2 S. Das and K. C. Mandal, *Nanocrystals*, 2013, **5**, 913.
3 P. Mukherjee, R. F. Sloan, C. M. Shade, D. H. Waldeck and S. Petoud, *J. Phys. Chem. C*, 2013, **117**, 14451.
4 S. Ye, S. Tanabe, N. Jiang and D. Wang, *Appl. Phys. B*, 2012, **108**, 553.
5 Q. Luo, X. S. Qiao, X. P. Fan and X. H. Zhang, *Opt. Lett.*, 2011, **36**, 2767.
6 C. Yan, A. Dadvand, F. Rosei and D. F. Perepichka, *J. Am. Chem. Soc.*, 2010, **132**, 8868.
7 P. Vergeer, T. J. H. Vlugt, M. H. F. Kox, M. I. Den Hertog, J. P. J. M. Vander Eerden and A. Meijerink, *Phys. Rev. B: Condens. Matter Mater. Phys.*, 2005, **71**, 014119.
8 Q. Y. Zhang, C. H. Yang, Z. H. Jiang and X. H. Ji, *Appl. Phys. Lett.*, 2007, **90**, 061914.
9 S. Ye, B. Zhu, J. X. Chen, J. Luo and J. R. Qiu, *Appl. Phys. Lett.*, 2008, **92**, 141112.
10 Q. H. Zhang, J. Wang, G. G. Zhang and Q. Su, *J. Mater. Chem.*, 2009, **19**, 7088.
11 G. J. Gao and L. Wondraczek, *Opt. Mater. Express*, 2013, **3**, 633.
12 G. J. Gao and L. Wondraczek, *J. Mater. Chem. C*, 2013, **1**, 1952.
13 V. Mahalingam, R. Naccache, F. Vetrone and J. A. Cobianco, *Opt. Express*, 2012, **20**, 111.
14 Y. S. Chang, H. J. Lin, Y. C. Li, Y. L. Chai and Y. Y. Tsai, *J. Solid State Chem.*, 2007, **180**, 3076.
15 T. Trupke, M. A. Green and P. Würfel, *J. Appl. Phys.*, 2002, **92**, 1668.
16 C. Strümpel, M. McCann, G. Beaucarne, V. Arkhipov, A. Slaoui, V. Švrček, C. del Cañizo and I. Tobiasd, *Sol. Energy Mater. Sol. Cells*, 2007, **91**, 238.